Mesoscale features and micronekton in the Mozambique Channel: An acoustic approach

Article *in* Deep Sea Research Part II Topical Studies in Oceanography · February 2014

DOI: 10.1016/j.dsr2.2013.10.024

6 authors, including:

Louis du Buisson
University of Cape Town
3 PUBLICATIONS **59** CITATIONS
SEE PROFILE

Erwan Josse
Institute of Research for Development
103 PUBLICATIONS **1,208** CITATIONS
SEE PROFILE

Anne Lebourges-Dhaussy
Institute of Research for Development
39 PUBLICATIONS **331** CITATIONS
SEE PROFILE

Frédéric Ménard
French National Research Institute for Sustai…
110 PUBLICATIONS **1,860** CITATIONS
SEE PROFILE

Deep-Sea Research II 100 (2014) 164–173

Contents lists available at ScienceDirect

Deep-Sea Research II

journal homepage: www.elsevier.com/locate/dsr2

Mesoscale features and micronekton in the Mozambique Channel: An acoustic approach

Nolwenn Béhagle [a,1], Louis du Buisson [a,b,c,*,1], Erwan Josse [a], Anne Lebourges-Dhaussy [a], Gildas Roudaut [a], Frédéric Ménard [b]

[a] Institut de Recherche pour le Développement (IRD), UMR LEMAR 195 (UBO/CNRS/IRD), Campus Ifremer, BP 70, 29280 Plouzané, France
[b] Institut de Recherche pour le Développement (IRD), UMR 212 EME (IRD/IFREMER/UM2), Avenue Jean Monnet, BP 171, 34203 Sète cedex, France
[c] Department of Biological Sciences and Marine Research Institute, University of Cape Town, Private Bag X3, Rondebosch 7701, Cape Town, South Africa

ARTICLE INFO

Available online 6 November 2013

Keywords:
Acoustics
Mesoscale eddies
Micronekton
Mozambique Channel
Satellite altimetry

ABSTRACT

The oceanic circulation in the Mozambique Channel (MZC) is dominated by mesoscale cyclonic and anticyclonic eddies that are known to play a key role in biological processes of less-productive deep-sea ecosystems by converting physical energy into trophic energy and by restructuring and concentrating biomass across the eddy field. In this study, hydroacoustics was used to investigate the spatial distribution of micronekton according to four classes of mesoscale features and assess whether cyclonic eddies, anticyclonic eddies or eddy edges (divergence and frontal regions) impact the density of micronekton. Acoustic data were collected continuously with a Simrad EK60 split-beam echosounder during three surveys carried out in the MZC within the framework of the MESOBIO programme. First, micronekton ascents and descents during the crepuscular periods (dusk and dawn, respectively) were similar to the well-known process of diel vertical migration, with the largest changes in the shallow layer, much smaller in the deep layer, and almost non-existent in the intermediate layer. Additionally, the acoustic densities for the total water column were greater at night than during the day, suggesting that organisms migrate from layers deeper than the water column that was sampled (740 m). Second, there was evidence of differences in the acoustic responses of micronekton to mesoscale features During two of the three surveys, cyclonic eddies exhibited greater micronekton density than anticyclonic eddies for day and night. In contrast, during the last survey, the greatest micronekton density was observed in anticyclonic eddies. To explain this discrepancy, several hypotheses are proposed, including the eddy generation site and trajectory throughout the life of the eddy, eddy-eddy interactions, seasonality and difference in monsoon wind regime, the depth of influence of eddies and a low dependence of movements of larger micronektonic organisms on the mesoscale gradients. Furthermore, this study demonstrated that mesoscale features could be predicted using acoustic responses at several acoustic frequencies.

1. Introduction

The Mozambique Channel (MZC) is located in the southwestern Indian Ocean between the east coast of Africa and the west coast of Madagascar and is characterised by important mesoscale activity (De Ruijter et al., 2002). The circulation in this area is dominated by mesoscale cyclonic and anticyclonic eddies that propagate southwards along the western edge of the channel (Schouten et al., 2003; Quartly and Srokosz, 2004). Mesoscale eddies can be characterised using different but complementary attributes such as rotational sense, dimension, intensity (e.g., sea surface height, geostrophic and rotational velocities), longevity, origin, trajectory, and propagation distance (Bakun, 2006; Chelton et al., 2011). In the MZC these mesoscale features have an average diameter of 300 km and may have a physical effect extending 1000–2000 m below the surface, but impact mainly the top 300 m of the water column (De Ruijter et al., 2004; Schouten et al., 2003; Ternon et al., 2013b).

Eddies play a key role in biological processes of less-productive deep-sea ecosystems by transferring physical energy of the ocean system into trophic energy by restructuring and concentrating biomass compared to the surrounding less-productive water (Bakun, 2006; Godø et al., 2012). Eddies can cause upwelling or downwelling in the centre and near the edges, depending on the rotational sense (clockwise and counter-clockwise respectively for

* Corresponding author at: Institut de Recherche pour le Développement (IRD), UMR LEMAR 195 (UBO/CNRS/IRD), Campus Ifremer, BP 70, 29280 Plouzané, France.
E-mail address: louis.dubuisson@ird.fr (L. du Buisson).
[1] These authors contributed equally to this work.

0967-0645/$ - see front matter © 2013 Elsevier Ltd. All rights reserved.
http://dx.doi.org/10.1016/j.dsr2.2013.10.024

cyclonic and anticyclonic eddies in the southern hemisphere). Cyclonic eddies are generally associated with divergent surface flows, leading to upwelling of nutrient-rich cold waters into the eddy centre (McGillicuddy et al., 1998; Bakun, 2006), causing an increase in local primary production (Mizobata et al., 2002; Benitez-Nelson et al., 2007; Tew-Kai and Marsac, 2009; Kolasinski et al., 2012). Anticyclonic eddies are generally associated with convergent horizontal surface movements, from the edges towards the centre of the eddy, which allow downwelling of organisms towards deeper layers in the centre (Bakun, 2006). Moreover, phytoplankton enrichment has also been associated with the upward movement of nutrient rich waters near the edges of either anticyclonic or cyclonic eddies (Mizobata et al., 2002; Quartly and Srokosz, 2004). A recent study of the MZC (Ternon et al., 2013b) supports these various aspects of the eddy dynamics. Several studies have analysed the links between mesoscale eddies and mesozooplankton or fish larvae (Bakun, 2006; Muhling et al., 2007), tunas (Bertrand et al., 1999; Young et al., 2001; Tew-Kai and Marsac, 2010), swordfish (Seki et al., 2002), turtles (Polovina et al., 2004; Lambardi et al., 2008), seabirds (Nel et al., 2001; Weimerskirch et al., 2004; Hyrenbach et al., 2006), and marine mammals (Bailleul et al., 2010). However, few studies have investigated the effect of mesoscale features on intermediate trophic levels, i.e. micronektonic organisms. Drazen et al. (2011) recently showed that eddies may aggregate micronekton, which probably feed on the enhanced secondary productivity associated with these eddies. Additionally, mesoscale features can shape the distribution and the aggregation patterns of micronekton through bottom-up processes (Sabarros et al., 2009).

In this study, hydroacoustic data was collected during three surveys carried out in the MZC in 2008, 2009 and 2010, within the framework of the MESOBIO programme (Ternon et al., 2013a). Hydroacoustics is a non-destructive and efficient method for continuously monitoring micronekton at large scales (Bertrand et al., 2003; Kloser et al., 2009). It is used in this study to (1) investigate the diel vertical migration pattern of micronekton, (2) test the influence of mesoscale features on micronekton density, and (3) predict mesoscale features using multi-frequency acoustic responses.

2. Methods

2.1. Acoustic data collection

Three oceanographic surveys were carried out in the MZC on board two research vessels. First, between 13–23°S and 35–43°E on the RV *Dr Fridtjof Nansen* (IMR, Norway) from 28 November–17 December 2008 (referred to here as MC08A). Second, between 23–26°S and 35–39°E on the RV *Antéa* (IRD, France) from 27 October–23 November 2009 (MC09B). Third, between 14–23°S and 39–43°E on the RV *Antéa* from 12 April to 6 May 2010 (MC10A) (Fig. 1).

In situ acoustic data was recorded continuously (day and night) at four frequencies (18, 38, 120, 200 kHz during MC08A; 38, 70, 120, 200 kHz during MC09B and MC10A) with a Simrad EK60 split-beam echosounder (Table 1). The depths of the hull-mounted acoustic transducers on the RV *Dr Fridtjof Nansen* and RV *Antéa* were approximately 5 and 3 m below the surface respectively. Acoustic data was processed with an offset of 10 m below the surface to account for the depths of the transducers and the acoustic interference from surface turbulence. The transducers were calibrated following standard procedures (Foote et al., 1987).

The water column was sampled vertically from the surface to a depth of 1000 m (MC08A) and 750 m (MC09B, MC10A). Data was recorded with the ER60 software (Simrad, 2008) ('*.raw' files) and converted into '*.hac' format for post-processing using 'Movies+' software (Weill et al., 1993). Settings used during data acquisition were basically the same for the three surveys, with only minor differences during the MC08A survey (Table 1) that, according to Korneliussen et al. (2008), do not impact the results. During the acquisition and processing of acoustic data, thresholds were applied to obtain the best signal/noise ratio, and transects were selected for processing according to several criteria, *i.e.* the optimal vessel speed, the nature of eddy crossed, the distance from the

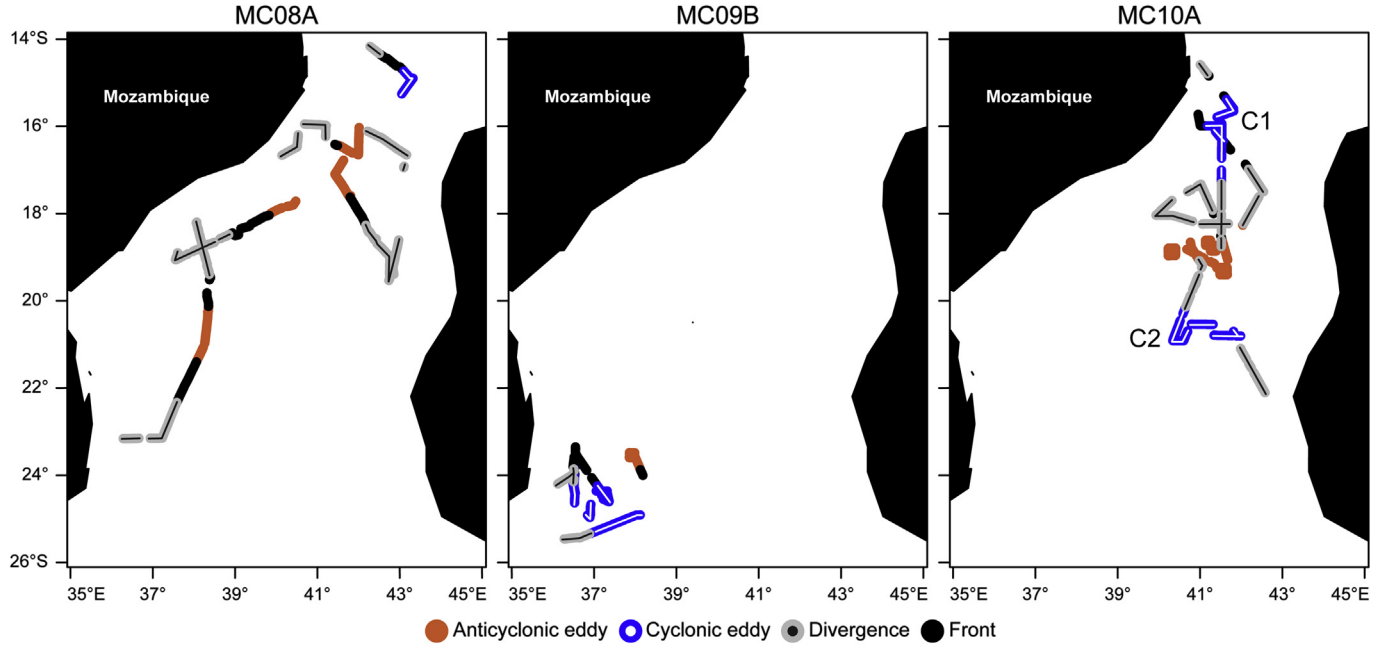

Fig. 1. Survey tracks (lines of dots) for cruises MC08A, MC09B and MC10A in the Mozambique Channel, with one dot per elementary sampling unit (ESDU): 1060 ESDUs for MC08A (28 November–17 December 2008), 491 ESDUs for MC09B (27 October–23 November 2009) and 1036 ESDUs for MC10A (12 April–6 May 2010). Dot colours indicate classes of mesoscale features. The locations of the stronger (C1) and weaker (C2) cyclones during MC10A are shown. (For interpretation of the references to colour in this figure caption, the reader is referred to the web version of this article.)

Table 1
Acoustic settings used with the Simrad EK60 split-beam echosounder during the three acoustics surveys (MC08A, MC09B, MC10A).

Survey	Frequency (kHz)	Ping rate (s^{-1})	Pulse length (s)	Power (kW)
MC08A	18	3–5	1.024×10^{-3}	2.00
	38	3–5	1.024×10^{-3}	2.00
	120	3–5	1.024×10^{-3}	0.25
	200	3–5	1.024×10^{-3}	0.12
MC09B and MC10A	38	1	5.120×10^{-4}	1.00
	70	1	5.120×10^{-4}	0.70
	120	1	5.120×10^{-4}	0.20
	200	1	5.120×10^{-4}	0.09

shore and the linearity of these transects. Although this implies that parts of the survey tracks were discarded, data processing and analyses were standardised across all three surveys.

2.2. Data analysis

2.2.1. Acoustic data processing

Movies+ was used for visual data control prior to processing, to assess the data quality and to remove noisy pings and bubble dropouts. During this inspection a minimal number of shoals and aggregations were observed, and therefore, echo-integration by layers (Simmonds and MacLennan, 2005) was applied during this study. Echo-integration by layers allows the quantification of the micronekton acoustic density of an area from the cumulative acoustic energy reverberated by all the targets in the zone sampled (Lurton, 2002). The minimum acquisition and echo-integration thresholds were respectively set at −80 and −75 decibels (dB). Following previous studies (e.g. Lebourges-Dhaussy et al., 2000; Ménard and Marchal, 2003; Sabarros et al., 2009), the elementary sampling distance unit (ESDU) was fixed at 1 nautical mile (nmi, 1 nmi=1852 m) in order to detect small-scale differences in acoustic responses across mesoscale features. The spatial autocorrelation in the acoustic data (i.e., spatial dependence between successive observations recorded along transects) was assessed and considered negligible, such as in Domokos (2009) and Sabarros et al. (2009). The water column was echo-integrated within 37 layers of 20 m depth, to a maximum depth of 740 m. These depth settings were used because the Movies+ software is limited to a maximum of 37 layers, the acoustic acquisition was limited to 750 m during the MC09B and MC10A surveys, and the micronekton acoustic intensity reduces considerably below 700 m. The Nautical Area Scattering Coefficient (NASC, s_A, $m^2\ nmi^{-2}$) (MacLennan et al., 2002) was used to determine the micronekton acoustic density. Assuming that the composition of the scattering layers and the resulting scattering properties of micronekton are relatively homogeneous, NASC can be used as a proxy of relative biomass of micronekton (e.g. Simmonds and MacLennan, 2005; Lawson et al., 2008), and NASC calculated from the 38 kHz acoustic frequency is representative of micronekton abundance (Bertrand et al., 1999).

To assess diel variation, diurnal and nocturnal periods were processed separately, and the crepuscular periods (dawn and dusk) corresponding to micronekton ascents and descents (Lebourges-Dhaussy et al., 2000; Benoit-Bird, 2009) were excluded from the analyses through visual analysis of the echograms. The times at which diel vertical migrations occurred varied considerably during dawn and dusk for MC08A (ranging between 23:10 and 05:30, and 12:00 and 17:50, respectively), MC09B (ranging between 01:00 and 03:45, and 14:00 and 18:10, respectively) and MC10A (ranging between 01:50 and 04:15, and 13:00 and 16:15, respectively). An initial analysis of the echograms indicated that organisms were organised vertically into three main layers. The water column was therefore separated into three layers: 10–200 m (surface layer, L_{200}, corresponding NASC s_{A1}), 200–400 m (intermediate layer, L_{400}, s_{A2}) and 400–740 m (deep layer, L_{740}, s_{A3}). Given the separation of the data into day/night surveys and into three vertical layers, and the vertical range limits of the transducers, micronekton density was analysed within six classes for 18 and 38 kHz, four for 70 kHz and two for 120 and 200 kHz frequencies. When investigating the global vertical distribution pattern, the 38 kHz frequency was used because it had the greatest vertical range limit of the frequencies common to all three surveys. The cruise path of each survey was divided into several linear transects according to time class (day versus night) and acoustic data quality (data without a large amount of acoustic interference). Transects close to the western continental shelf of the MZC (bathymetry less than 1500 m) were removed from the analyses because mesoscale features that interacted with the shelf had a significant impact on water mass properties (Lamont et al., 2013) and the acoustic responses.

2.2.2. Environmental data

Satellite altimetry allows identification of mesoscale features (e.g., Chelton et al., 2007). One mesoscale feature among four classes (A: anticyclone, C: cyclone, D: divergence, F: fronts) was assigned to each ESDU. The classification of each ESDU was processed using three explanatory variables (sea surface height anomaly, geostrophic current speed and bathymetry) and a discriminant function estimated from an extra training dataset (Lamont et al., 2013). Ocean bathymetry was extracted from ETOPO1 Global Topography (data access: ⟨http://www.ngdc.noaa.gov/mgg/global/global.html⟩). Sea level anomaly and the corresponding geostrophic speed were extracted from AVISO products "DT-MSLA Ref" (Delayed Time, DT; Reference, Ref) with $0.33 \times 0.33^{\circ}$ spatial resolution on a Mercator grid. The predictions from the linear discriminant analysis were estimated for each ESDU using the values taken by the three explanatory variables at the corresponding temporal and spatial positions. In general, cyclonic features were associated with large negative sea surface height anomalies (SSHA) and slower geostrophic current speeds (GC) compared to anticyclonic features that had large positive SSHA and slightly faster GC. Divergence features typically had small SSHA and slow GC, while frontal stations had small SSHA and fast GC. Fig. 2 depicts the differences in the SSHA and GC assigned to the ESDUs of the three surveys.

2.2.3. Statistical analysis

Links between acoustic density estimates (s_A) representing the vertical distribution of micronekton, period of the day, depth layers (L_{200}, L_{400}, and L_{740}), and mesoscale features, were investigated using multivariate analysis of variance (MANOVA), non-parametric Kruskal–Wallis (KW) tests and pairwise Wilcoxon rank sum tests.

Multinomial models (from the Generalized Linear Model family) were applied to quantify the link between classes of mesoscale features and acoustic responses for each survey. The vector of predicted class of mesoscale feature (Y_i, $i \in [1, N]$, with N=total number of ESDUs) was assumed to be a realisation of a random variable Y. Y takes its values in the set E={A, C, D, F} of four categories. The model was designed in terms of the probability function of Y, conditional to the acoustic responses in the three layers: $(s^f_{A1})_i$ for the common frequencies f=38, 120 and 200 kHz in the surface layer, and $(s^{38kHz}_{A2})_i$ and $(s^{38kHz}_{A3})_i$ in the intermediate and deep layers respectively. The number of covariates assessed per model was dependent on the maximum depth range of each acoustic frequency (38 kHz: s_{A1}, s_{A2} and s_{A3}; 120 and

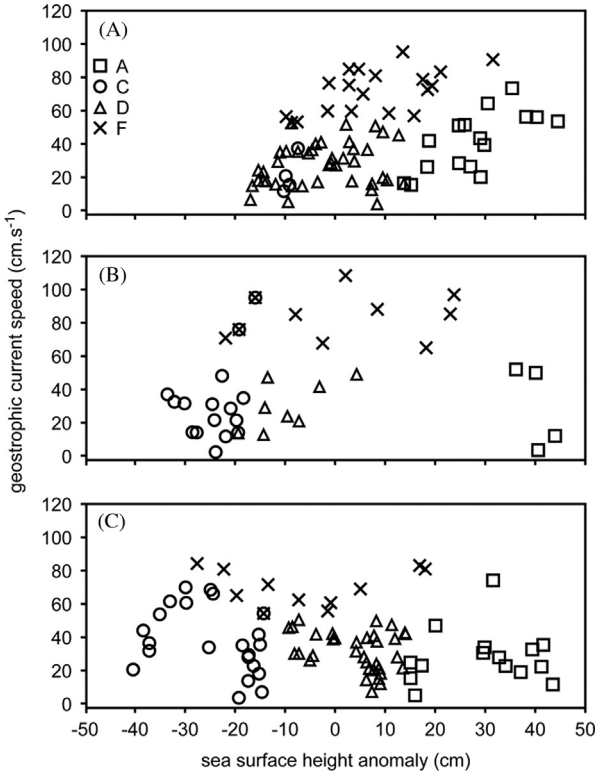

Fig. 2. Geostrophic current speed (GC) versus sea surface height anomalies (SSHA) associated with elementary sampling units (ESDUs) along the tracks of the three surveys (see text): (A) MC08A, (B) MC09B, (C) MC10A; and corresponding mesoscale classes (A, anticyclone; C, cyclone; D, divergence; F, front).

200 kHz: s_{A1}). The surface layer of the 200 kHz frequency refers to 10–140 m due to the sound absorption at the chosen echo-integration threshold. For $j \in E$, the probability distribution (Pr) is written:

$$\Pr(Y_i = j | (s_{A1}^{38kHz})_i = x_1^{38kHz}, (s_{A1}^{120kHz})_i = x_1^{120kHz}, (s_{A1}^{200kHz})_i = x_1^{200kHz}, (s_{A2}^{38kHz})_i = x_2, (s_{A3}^{38kHz})_i = x_3) = g\left(\lambda_j + \sum_f \beta_1^f x_1^f + \beta_2 x_2 + \beta_3 x_3\right) \quad (1)$$

where g is the logistic function and λ_j, β_1^f, β_2, β_3 are the eight unknown parameters to be estimated. Day and night datasets were investigated separately. The Akaike Information Criterion (AIC) was used to select the covariates s_{A1}^f, s_{A2}^{38kHz} and/or s_{A3}^{38kHz} of the most parsimonious models. Reference models including SSHA and GC as covariates were also fitted and matched to the selected model based on acoustic responses only. In addition, estimated probabilities from eq. (1) permitted the prediction of the most likely mesoscale feature class from the acoustic responses. Predicted classes were then matched with the originally assigned mesoscale feature classes, and a global score of correct classification was computed for each model. Statistical analyses were conducted with R (R Development Core Team, 2007) using the *multinom* function in the MASS package (Venables and Ripley, 2002).

3. Results

A total of 2587 ESDUs combining data from the three surveys (Table 2) were processed following three steps. Firstly, a preliminary analysis examined the altimetry characteristics of the sampled features. Then, differences in the vertical distribution of micronekton between day and night, and among surveys, were investigated.

Table 2
Number of elementary sampling units (ESDUs, 1 nautical mile) for the three surveys (MC08A, MC09B, MC10A), the time period (day and night) and the mesoscale features (A, anticyclonic; C, cyclonic; D, divergence; F, front).

Survey	Total	Time period		Eddy class			
		Day	Night	A	C	D	F
MC08A	1060	531	529	237	45	543	235
MC09B	491	292	199	154	179	56	102
MC10A	1036	500	536	252	272	447	65
Total	2587	1323	1264	643	496	1046	402

Finally, the effect of mesoscale features on micronekton density was explored.

3.1. SSHA and GC characteristics of the mesoscale features

The sampling of each feature was not balanced (Table 2). The SSHA and GC varied among the three surveys (Fig. 2). The mean ± s.d. SSHA of anticyclones sampled during MC08A and MC10A (28 ± 8 cm and 29 ± 11 cm respectively) were of a similar magnitude but significantly weaker than during MC09B (39 ± 2 cm, pairwise Wilcoxon rank sum tests, $p < 0.05$). The GC of anticyclones sampled during MC09B and MC10A (29 ± 23 cm s^{-1} and 28 ± 16 cm s^{-1} respectively) were significantly slower than during MC08A (41 ± 16 cm s^{-1}, pairwise Wilcoxon rank sum tests, $p < 0.05$). The cyclone sampled during MC08A (SSHA: −9 ± 1 cm; GC: 21 ± 7 cm s^{-1}) was weaker than those sampled during MC09B (SSHA: −24 ± 5 cm; GC: 34 ± 26 cm.s^{-1}) and MC10A (SSHA: −25 ± 9 cm; GC: 36 ± 17 cm s^{-1}) (both significant pairwise Wilcoxon rank sum tests, $p < 0.05$). However, the MC10A survey sampled two contrasting cyclones: the cyclone at the MZC narrows (C1, ~16°S, Fig. 1) had the greatest SSHA and GC values of all three surveys, whereas the southern cyclone (C2, ~20–21.5°S, Fig. 1) had intermediate values between the cyclone sampled during MC08A and the cyclones sampled during MC09B. The GC ranged from 2 cm s^{-1} in the centre of the eddies to 108 cm s^{-1} in the frontal regions between the eddies.

3.2. Diel vertical distribution of micronekton

Micronekton vertical distribution varied between day and night according to the diel vertical migration patterns. KW tests and pairwise Wilcoxon rank sum test comparisons between layers (L_{200}, L_{400}, L_{740}) performed on day and night data showed that acoustic responses of the 38 kHz frequency differed significantly between the three layers ($p < 0.001$ each). Based on the 38 kHz frequency, the acoustic densities in the deep layer during the day (> 70% of the water column) and the surface layer during the night (> 60% of the water column) were similar (Fig. 3). However, acoustic densities in the deep layer during the night remained relatively high (half that recorded in the surface layer), and the acoustic densities of the total water column were more than 20% greater during the night than during the day. Acoustic density increased by an average 79% between day and night in the shallow layer and decreased by 46% in the deep layer. Day and night acoustic densities in the intermediate layer were less than 7% of the total water column and increased by 20% (MC08A and MC09B) or decreased by 30% (MC10A) between day and night. Furthermore, there were differences in the global micronekton densities among surveys (Fig. 3). Day and night acoustic densities estimated during MC08A were greater than the other two surveys (from 20% to 31% depending on the time period and survey), while MC09B and MC10A exhibited acoustic densities of a similar magnitude (day difference of 10%; night difference of 4%).

3.3. Link between mesoscale features and micronekton density

MANOVA tests performed by survey and by time period (day and night) for the 18, 38 and 70 kHz frequencies (i.e. frequencies allowing characterisation of several layers) showed that the overall acoustic densities of the three depth layers differed significantly among mesoscale features ($p < 0.001$ each). KW tests were applied to each layer to test for differences in acoustic densities among mesoscale features during day/night periods, at each acoustic frequency (Table 3). Most of the tests were significant, except for the day-time shallow layer (L_{200}) of MC08A at 18 kHz, the day-time deep layer (L_{740}) and night-time intermediate layer (L_{400}) of MC08A at 38 kHz, the day-time intermediate layer (L_{400}) of MC10A at 38 kHz, and the day-time shallow layer (L_{200}) of MC10A at 120 kHz. However, as previously shown, the proportion of acoustic density recorded in the intermediate layers was small relative to the overall acoustic density during both day and night (Fig. 3). Therefore, mainly the dominant layers were considered henceforward, i.e. the deep layer (L_{740}) during the day and the surface layer (L_{200}) during the night, and for the frequencies common to all surveys (38, 120 and 200 kHz) only.

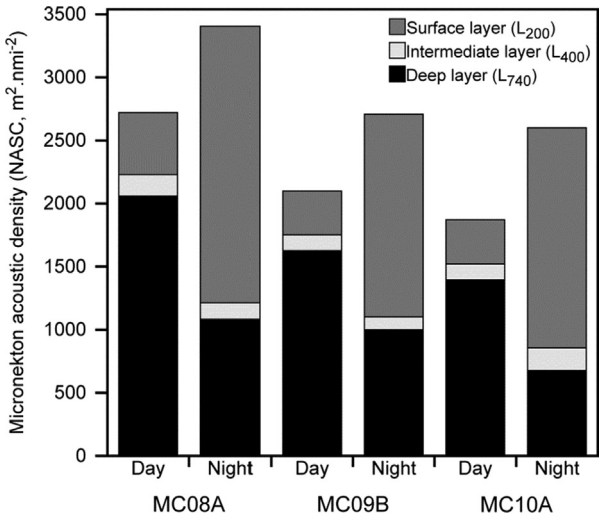

Fig. 3. Micronekton acoustic density estimates (Nautical Area Scattering Coefficient, 38 kHz echosounder frequency) during the day and night, for the three surveys (MC08A, MC09B, MC10A), and contribution by depth layer (L_{200}, the surface layer, 10–200 m; L_{400}, the intermediate layer, 200–400 m; and L_{740}, the deep layer, 400–740 m).

During the day, at the 38 kHz frequency, cyclonic eddies sampled during the MC08A and MC09B surveys exhibited greater average acoustic density in the deep layer (L_{740}) than anticyclones (mean ± s.d. = 2252 ± 364 versus 1933 ± 166 m^2 nmi^{-2} for MC08A; 1980 ± 486 versus 1382 ± 59 m^2 nmi^{-2} for MC09B) (Fig. 4A). However, the acoustic densities of the MC08A survey were not significantly different during the day, while for MC09B, the acoustic densities were significantly different between cyclonic and anticyclonic eddies (Fig. 4A). Moreover, anticyclones did not differ from fronts, and cyclones did not differ from divergences during MC09B. The MC10A survey exhibited a different pattern during the day (Fig. 4A), with anticyclones not significantly different from divergences, and both classes exhibiting greater acoustic densities on average (1617 ± 262 and 1520 ± 497 m^2 nmi^{-2} respectively) than cyclones (1138 ± 333 m^2 nmi^{-2}) and fronts (1066 ± 696 m^2 nmi^{-2}). In addition, acoustic density did not differ significantly between cyclones and fronts on the one hand, and between fronts and divergences on the other hand.

A similar trend was observed during the night in the surface layer (L_{200}) for the MC08A and MC09B surveys. Anticyclones exhibited lower average acoustic densities (1702 ± 431 and 1264 ± 223 m^2 nmi^{-2} respectively) than cyclones (2541 ± 535 and 1983 ± 680 m^2 nmi^{-2} respectively), divergences (2350 ± 825 and 1754 ± 459 m^2 nmi^{-2} respectively) and fronts (2145 ± 734 and 1717 ± 436 m^2 nmi^{-2} respectively), which did not differ significantly from each other (Fig. 4B). MC10A exhibited a different pattern again, with mean acoustic densities of anticyclones (1735 ± 464 m^2 nmi^{-2}) significantly greater than cyclones (1273 ± 539 m^2 nmi^{-2}) and fronts (1366 ± 662 m^2 nmi^{-2}), and significantly lower than divergences (2059 ± 677 m^2 nmi^{-2}) (Fig. 4B).

Table 3
Kruskal–Wallis (KW) comparison tests of the micronekton densities (s_A, m^2 nmi^{-2}) between the mesoscale feature classes, by depth layers (L_{200}, surface layer, 10–200 m; L_{400}, the intermediate layer, 200–400 m; L_{740}, the deep layer, 400–740 m), by time period (day and night), and for the three surveys (MC08A, MC09B, MC10A). Statistical tests are presented as Chi-squared ($\chi^2_{df=3}$) and *p*-values.

Frequency (kHz)	**Period**	**Survey**	**MC08A**		**MC09B**		**MC10A**	
		Depth layer	$\chi^2_{df=3}$	***p*-value**	$\chi^2_{df=3}$	***p*-value**	$\chi^2_{df=3}$	***p*-value**
18	Day	L_{200}	3.180	0.365	–	–	–	–
		L_{400}	80.900	< 0.001	–	–	–	–
		L_{740}	32.459	< 0.001	–	–	–	–
	Night	L_{200}	84.047	< 0.001	–	–	–	–
		L_{400}	24.561	< 0.001	–	–	–	–
		L_{740}	40.343	< 0.001	–	–	–	–
38	Day	L_{200}	8.161	0.043	101.102	< 0.001	50.855	< 0.001
		L_{400}	84.872	< 0.001	79.033	< 0.001	6.949	0.074
		L_{740}	5.667	0.129	76.797	< 0.001	117.214	< 0.001
	Night	L_{200}	92.534	< 0.001	96.924	< 0.001	132.537	< 0.001
		L_{400}	1.964	0.580	53.965	< 0.001	76.219	< 0.001
		L_{740}	30.774	< 0.001	61.289	< 0.001	87.857	< 0.001
70	Day	L_{200}	–	–	21.688	< 0.001	17.164	0.001
		L_{400}	–	–	130.560	< 0.001	33.444	< 0.001
	Night	L_{200}	–	–	75.782	< 0.001	161.071	< 0.001
		L_{400}	–	–	87.397	< 0.001	78.542	< 0.001
120	Day	L_{200}	33.698	< 0.001	117.188	< 0.001	5.052	0.168
	Night	L_{200}	129.986	< 0.001	117.973	< 0.001	118.119	< 0.001
200	Day	L_{200}	58.839	< 0.001	150.454	< 0.001	47.785	< 0.001
	Night	L_{200}	203.711	< 0.001	115.293	< 0.001	101.137	< 0.001

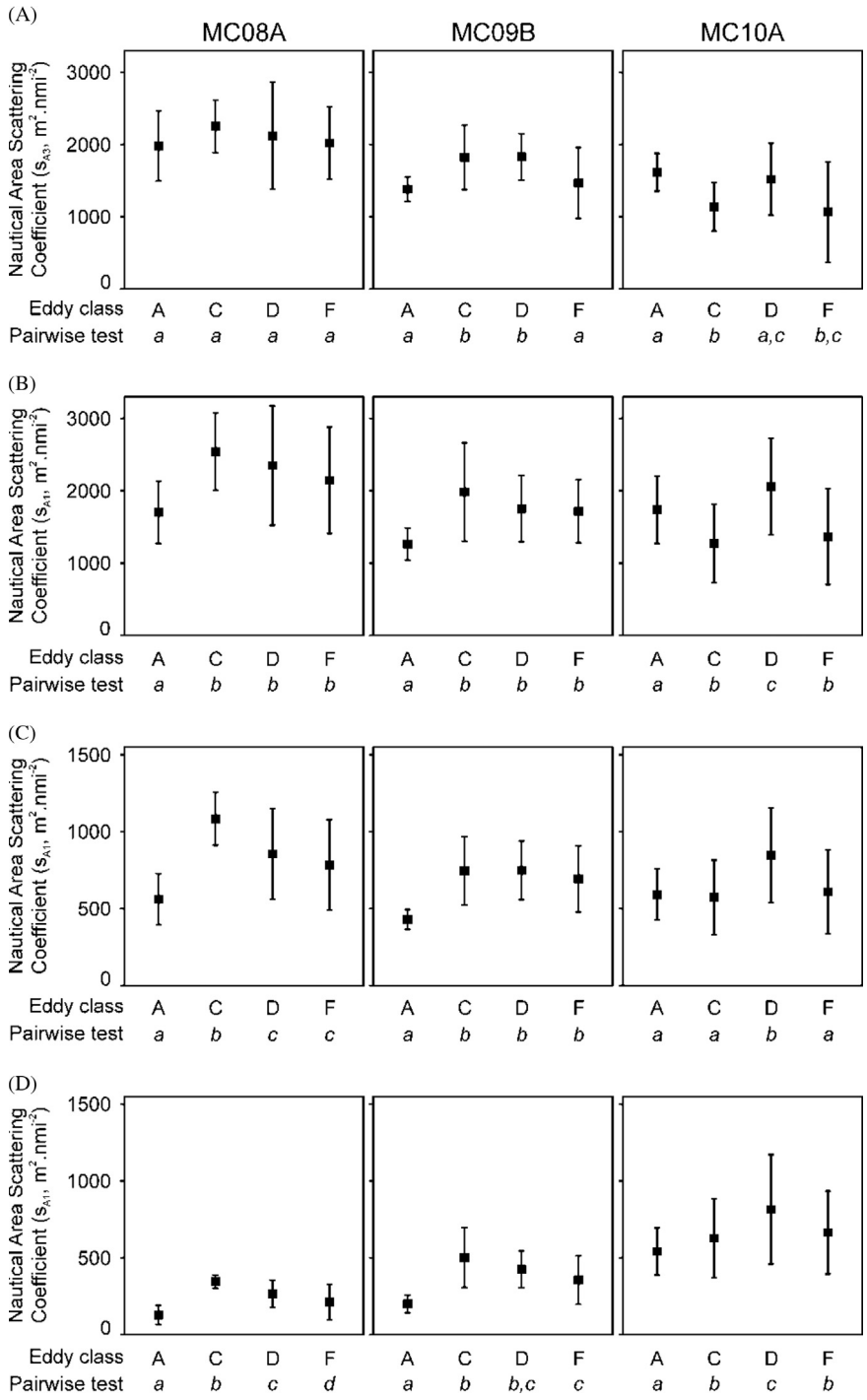

Fig. 4. Mean (points) and standard deviation (error bars) of acoustic densities of micronekton (Nautical Area Scattering Coefficient) according to mesoscale class (A, anticyclone; C, cyclone; D, divergence; F, front) in (A) the deep layer L_{740} (400–740 m) for day data at 38 kHz, (B) the surface layer L_{200} (10–200 m) for night data at 38 kHz, (C) the surface layer L_{200} (10–200 m) for night data at 120 kHz, and (D) the surface layer L_{200} (10–140 m) for night data at 200 kHz, for the three surveys (MC08A, MC09B, MC10A). Note that the *y*-axis scales of (C) and (D) are half those of (A) and (B). Lowercase lettering indicates mesoscale features that were not significantly different according to pairwise Wilcoxon rank sum tests (Pairwise test).

The results obtained with the 120 and 200 kHz frequencies in the shallow layer (L_{200}) during the night showed the same overall pattern as the 38 kHz frequency for the MC08A and MC09B surveys (Fig. 4). Differences among the mesoscale features were generally more distinct and significantly different for the 120 and 200 kHz (Table 3), although acoustic densities were 8–49% of those detected at 38 kHz. However, during the MC10A survey, mean acoustic densities of anticyclones did not differ from cyclones and fronts for the 120 kHz, while anticyclones were significantly lower than the other features for the 200 kHz (Fig. 4). For both frequencies, divergences displayed the highest significant acoustic densities once more. Although not presented here, the results obtained with the 18 kHz (L_{200}, night and L_{740}, day for MC08A) and 70 kHz (L_{200}, night for MC09B and MC10A) frequencies showed the same patterns as the 120 kHz frequency. However, at the 18 kHz frequency, acoustic densities in the night-time shallow

Table 4
Multinomial models with (1) sea surface height anomaly (SSHA) and geostrophic current speed (GC) and (2) micronekton densities (Nautical Area Scattering Coefficient, $m^2\ nmi^{-2}$) of the surface layer (10–200 m depth, s_{A1}), intermediate layer (200–400 m depth, s_{A2}) and deep layer (400–740 m depth, s_{A3}) at the 38 kHz frequency, and of the surface layer at the 120 and 200 kHz frequencies, as covariates. Due to the depth limits of the transducers, the surface layer at the 200 kHz frequency refers to 10–140 m depth. Results are given in terms of Akaike Information Criterion (AIC) and scores of correct classification of mesoscale eddy classes (%).

	Covariates	MC08A	MC09B	MC10A
Day	SSHA, GC	158 (96%)	34 (99%)	18 (100%)
	38 kHz, 120 kHz, 200 kHz	1107 (57%)	361 (80%)	701 (74%)
Night	SSHA, GC	203 (95%)	70 (93%)	30 (100%)
	38 kHz, 120 kHz, 200 kHz	573 (83%)	317 (75%)	929 (70%)

layer were one to two times greater than at 38 kHz, and there was no significant difference between anticyclones and cyclones in the day-time deep layer.

All multinomial model configurations selected the five acoustic responses, $s_{A1}^{38kHz}, s_{A2}^{38kHz}, s_{A3}^{38kHz}, s_{A1}^{120kHz}, s_{A1}^{200kHz}$, as covariates of the final models. Results are given in terms of Akaike Information Criterion (AIC) and scores of correct classification (%) of mesoscale feature classes (Table 4). Reference models, using SSHA and GC, obtained considerably lower AIC values than models based on acoustic responses, and reference models logically obtained outstanding classification scores. Conversely, models based on acoustic responses displayed varying scores. The night-time MC08A survey exhibited the highest classification score of 83% based mainly on correct classifications of anticyclones and divergences. However, the day-time MC08A survey exhibited the lowest score of 57%, based mainly on correct classifications of divergences and fronts, and with no correct classifications of cyclones. The day- and night-time scores of MC09B (80% and 75%, respectively) were greater than the MC10A scores (74% and 70%, respectively).

4. Discussion

This study demonstrated that the vertical and horizontal distribution of micronekton in the MZC is influenced by the circadian rhythm (Fig. 3) and mesoscale dynamics (Fig. 4) respectively. We also demonstrated that mesoscale features can be predicted using acoustic responses of micronekton recorded at several frequencies. However, the links between mesoscale features (anticyclones, cyclones, divergences and fronts) and acoustic responses of micronekton, measured as Nautical Area Scattering Coefficient (s_A, $m^2\ nmi^{-2}$) and referred to here as acoustic densities, were not consistent from one survey to another. Although the combination of remote sensing and acoustic technologies lead to the detection of differences in micronekton acoustic densities at the mesoscale, further investigation and additional data is required to distinguish more robust patterns and to provide information about the underlying ecological processes that generate our observations. Hypotheses are proposed below to support the results, taking into account the sampling methods and the special nature of the data used in this study.

4.1. Diel vertical distribution of micronekton

The majority of the acoustic responses detected during this study are attributed to migratory micronekton that typically occur in the upper 200 m of the water column at night and migrate below 400 m during the day (Fig. 3). Although the MZC is a relatively narrow channel highly influenced by topography, island effects and highly variable mesoscale eddy features, micronekton ascents and descents during the crepuscular periods (dusk and dawn respectively) in this investigation were similar to the well-known process of diel vertical migration (e.g., Lebourges-Dhaussy et al., 2000; Benoit-Bird, 2009; Domokos, 2009; Godø et al., 2009; Drazen et al., 2011; Godø et al., 2012), with the largest changes in the shallow layer, much smaller changes in the deep layer, and almost non-existent changes in the intermediate layer. Additionally, the acoustic densities for the total water column were greater at night than during the day, suggesting that organisms migrate from layers deeper than 740 m (beyond the range of the 38 kHz transducer), as observed previously in the tropical Pacific Ocean (e.g. Roger and Grandperrin, 1976; Domokos, 2009) and in the North Atlantic Ocean (Godø et al., 2009; Godø et al., 2012). Furthermore, some organisms may not ascend during dusk but reside in the same habitat during the night, as already described for pelagic fishes (Watanabe et al., 1999), squids (Watanabe et al., 2006) and micronekton (Domokos, 2009). Indeed, resident and migrant strategies can co-exist in some populations, and the factors affecting migration can be multifaceted and plastic responses (Olsson et al., 2006; Mehner and Kasprzak, 2011). Multi-frequency acoustic analyses based on several transducers processed at finer ESDU sizes than the present study could provide information on these complex patterns, especially for investigating the migration processes during the crepuscular periods.

4.2. ESDU classification and spatial resolution

Mesoscale features were assigned to acoustic ESDUs using data extracted from satellite altimetry and a discriminant function analysis (Lamont et al., 2013). The ESDU was fixed at 1 nmi, while the satellite data (SSHA and the corresponding GC) were merged datasets and model outputs produced by AVISO, with a larger spatial resolution of about 0.33°, corresponding to approximately 40 km (Chelton et al., 2011). SSHA fields from satellite altimetry reveal mesoscale features, but the resolution of altimetry data is too large to match an accurate tracking of the processes recorded by acoustics at small spatial scales. The mesoscale feature classification approach was used to discriminate between anticyclone, cyclone, divergence and frontal areas. As described by Lamont et al. (2013), divergences and fronts were characterised by slow and fast GCs, respectively, and by small SSHAs (Fig. 2). The separation between divergence and frontal areas can be blurred, and additional information would allow for further investigation. Nevertheless, this approach was a suitable compromise permitting an objective assignment of mesoscale feature class, using an efficient way of identifying mesoscale features in the field.

4.3. Link between mesoscale features and micronekton density

The nature of eddies, especially cyclonic and/or anticyclonic eddies, has been suggested to impact the distribution of marine organisms through bottom-up effects (e.g., Seki et al., 2002; Muhling et al., 2007; Domokos et al., 2007; Sabarros et al., 2009; Bailleul et al., 2010; Gruber et al., 2011; Godø et al., 2012). Cyclonic eddies are generally characterised by nutrient-rich water in the euphotic zone that triggers primary production (McGillicuddy and Robinson, 1997; Bakun, 2006; Muhling et al., 2007). Low primary production is usually associated with anticyclones but enrichments have been reported at their periphery (Franks et al., 1986; Mizobata et al., 2002). In addition, contra-rotating eddy pairs, referred to as dipoles, generate important energetic fronts, causing the accumulation of biological material with the formation of filaments (Tew-Kai and Marsac, 2009). Cyclonic eddies sampled during MC08A and MC09B showed greater micronekton acoustic densities than anticyclonic eddies during the day and night

(Fig. 4). All tests were significantly different except for the deep layer of the day dataset of MC08A (Table 3). Contrary to initial expectation, acoustic densities were greater in anticyclonic than cyclonic eddies during the MC10A survey. Similar contrasts were observed with a Tracor acoustic profiling sensor (TAPS) used to acoustically investigate the influences of mesoscale features on zooplankton (Lebourges-Dhaussy et al., 2013); the biovolume integrated over 0–200 m of the largest size-class analysed (1–3 mm) was greater in cyclonic than anticyclonic eddies during MC09B, and vice versa during MC10A. This particular finding, from different acoustic records of the MC10A survey only, contradicts the overall paradigm that biological production is greater in cyclonic eddies compared to anticyclonic eddies (e.g. Zimmerman and Biggs, 1999; Goldthwait and Steinberg, 2008; Landry et al., 2008; Huggett, 2013). But biological responses can become more complex due to several interacting factors, such as the location where eddies began spinning up, the interactions between them and the distance from the shelf. For instance, anticyclonic eddies can develop higher phytoplankton biomass inside the eddy as upwelling outside the eddy can increase phytoplankton concentrations that can then be advected into the eddy (Kim et al., 2011). Such influence on the transport and distribution of nutrients obviously impacts the spatial structure of the base of the food web, and also affects the distribution of upper trophic level organisms (e.g. Strzelecki et al., 2007). The contrasting biological responses between micronekton acoustic densities in cyclones and anticyclones in the present study may be related to specific environmental conditions, which are described below.

4.3.1. Wind stress

Wind-forcing can lead to anomalously higher chlorophyll concentrations inside anticyclonic eddies compared to those expected from classic eddy pumping (Siegel et al., 2011) and can amplify the phytoplankton biomass in mode-water eddies and reduce upwelling in cyclonic eddies (McGillicuddy et al., 2007). The expected eddy dynamics of the MZC may therefore be influenced by the monsoon wind regime of the western Indian Ocean (Schott and McCreary, 2001). However, the monsoonal winds influence mainly the northern MZC (Ramage, 1969; Bigg, 1992). In addition, the variability in sample locations of the present study and the high variability in wind speed and direction on daily timescales (Ternon et al., 2013b) blur the differences in wind patterns among the three surveys. Therefore, although it can play a key role, wind-forcing cannot be considered as the main process leading to greater micronekton acoustic densities in anticyclones compared to cyclones.

4.3.2. Eddy life history and interactions

The age of eddies, the location where eddies began spinning up, their trajectory, and eddy-eddy interactions appears to have a major influence on the biological responses of the eddy fields in the MZC (Bakun, 2006; Chelton et al., 2011; Halo et al., 2013; José et al., 2013; Lamont et al., 2013; Malauene et al., 2013; Ternon et al., 2013b). Indeed, the three surveys did not sample the same pattern of eddies. In 2009 (MC09B), a stable and mature anticyclonic/cyclonic dipole, which formed two months prior to the survey (Ternon et al., 2013b), was sampled near to the Mozambique coast in the south-western MZC. In contrast, in 2008 (MC08A) and 2010 (MC10A) the suites of eddies sampled throughout the Channel were in their early stages and unstable, respectively. In addition, the eddy field of the MC10A survey differed due to (1) a large cyclonic eddy at the narrows of the MZC (C1, ~16°S, Fig. 1) with dynamical characteristics (amplitude, edge velocity and vertical structure) comparable to anticyclones usually formed at this location, and (2) a less structured eddy field in the south of the Channel (Ternon et al., 2013b). Although the atypical C1 was the strongest cyclone (greatest SSHA and GC values) sampled during all three surveys, the micronekton densities in the dominant layers (day-time deep and night-time surface layers) were 40% less than the weak MC10A southern cyclone (C2, Fig. 1) and the least out of all cyclones sampled during the two other surveys. Surprisingly, the micronekton densities recorded in the day-time surface layer of C1 contributed strongly to the total acoustic density, suggesting that the surface layers of C1 may have consisted of a greater proportion of smaller, non-migratory organisms than in the other cyclones. This hypothesis is supported by TAPS observations that show a relatively higher proportion of smaller organisms in the upper 25 m than in the deeper layers of C1 (Lebourges-Dhaussy et al., 2013). The lower than expected micronekton densities within the atypical C1, combined with the relatively weak C2, may explain the unexpected greater acoustic density detected in anticyclones compared to cyclones in MC10A.

4.3.3. Hydrological context

MC10A exhibited different hydrological properties compared to the two previous surveys, with lower mean temperatures at 100 m, shallower nitracline depths in frontal regions and lower salinity in divergence regions (Lamont et al., 2013). During MC10A the frontal zone of the energetic cyclone C1 interacted with the continental shelf, causing intensified currents and upwelling of colder water near the narrows, whereas during MC08A and MC09B, similar interaction occurred with anticyclonic eddies near the narrows and southwestern MZC respectively. The proximity of an eddy to the shelf can lead to entrainment of nutrients into the eddy (Tew-Kai and Marsac, 2009; José et al., 2013; Roberts et al., 2013; Lamont et al., 2013). Intense upwelling and nutrient entrainment on the western edge of the atypical cyclone C1 during MC10A may have led to the divergences exhibiting the greatest micronekton densities in the surface layer. Additionally, elevated levels of phyto- and zooplankton biomass may also have been advected into anticyclonic eddies through convergence. Therefore, the greater micronekton densities in anticyclonic compared to cyclonic eddies during MC10A may possibly be attributed to proximity to the continental shelf.

4.3.4. Mobility of organisms

The influence of eddies may be blurred by the mobility of micronekton during diel vertical migrations. The effects of mesoscale features are more intense in the upper 300 m (De Ruijter et al., 2004; Schouten et al., 2003), while the effects of currents are evident to depths of 500 m in anticyclones and 100 m in cyclones (Ternon et al., 2013b). Micronekton organisms that migrate below 400 m at dawn may be located half of the time in water masses weakly impacted by eddies. Assuming that eddies may impact mainly surface waters only, we examined the day-time shallow layer (L_{200}) again and compared the acoustic densities of the non-migratory organisms among cyclones and anticyclones. Cyclones remained acoustically richer than anticyclones for MC08A and MC09B, as did cyclonic eddies during MC10A that exhibited, on average, 30% greater acoustic densities than anticyclonic eddies. Migration strategy, however, dominates in the micronekton community compared with resident behaviour that can be related to peculiar species composition and/or size distributions more influenced by mesoscale dynamics. In addition, Ménard et al. (2013) and Potier et al. (2013) suggest that micronekton may not necessarily be trapped within particular features because they have the ability to swim across eddies in the MZC. The unexpected high micronekton densities in anticyclones of MC10A may therefore

be related to larger, more mobile organisms, which are less influenced by mesoscale features.

5. Conclusion

Biogeochemical and biological responses to mesoscale features of the components of the food web up to mid-trophic micronekton may be quite variable and the underlying mechanisms are complex to understand. Despite these complex interactions, this study improves the understanding of the impact of circadian rhythm and mesoscale eddies on the distribution of this important mid-trophic component, and illustrates that investigating factors that shape the distribution of micronekton is an important step towards understanding the relationship between physical oceanography and biological compartments in pelagic ecosystems. Acoustic techniques (including multi-frequency approaches) that allow direct monitoring of ecosystems at different spatiotemporal scales, are efficient tools that should lead to considerable progress in our knowledge of ecosystem functioning.

Acknowledgments

This work was mainly supported by the MESOBIO project that was funded by WIOMSA (MASMA grant 2009-2011). IRD (France), Department of Environment Affairs (South Africa), ASCLME and SWIOFP also funded this work. The research was supported by ANR project number 09-CEPL-0003 MACROES. LDB was financially supported by the South African National Research Foundation (NRF), the University of Cape Town, and the IRD through the International Centre for Education, Marine and Atmospheric Sciences over Africa (ICEMASA). The authors thank IRD colleagues Patrice Brehmer, Dominique Dagorne, Hervé Demarcq, Jean-François Ternon and Pascal Cotel for support and suggestions. We finally thank the referees for their contribution to the improvement of the manuscript.

References

Bailleul, F., Cotté, C., Guinet, C., 2010. Mesoscale eddies as foraging area of a deep-diving predator, the southern elephant seal. Mar. Ecol. Prog. Ser. 408, 251–264.
Bakun, A., 2006. Fronts and eddies as key structures in the habitat of marine fish larvae: opportunity, adaptive response and competitive advantage. Sci. Mar. 70S2, 105–122.
Benitez-Nelson, C.R., Bidigare, R.R., Dickey, T.D., Landry, M.R., Leonard, C.L., Brown, S.L., Nencioli, F., Rii, Y.M., Maiti, K., Becker, J.W., Bibby, T.S., Black, W., Cai, W.J., Carlson, C. A., Chen, F., Kuwahara, V.S., Mahaffey, C.M., McAndrew, P.M., Quay, P.D., Rappé, M.S., Selph, K.E., Simmons, M.P., Yang, E.J., 2007. Mesoscale eddies drive increased silica export in the subtropical Pacific Ocean. Science 136, 1017–1021.
Benoit-Bird, K.J., 2009. Dynamic 3-dimensional structure of thin zooplankton layers is impacted by foraging fish. Mar. Ecol. Prog. Ser. 396, 31–76.
Bertrand, A., Le Borgne, R., Josse, E., 1999. Acoustic characterisation of micronekton distribution in French Polynesia. Mar. Ecol. Prog. Ser. 191, 127–140.
Bertrand, A., Josse, E., Bach, P., Dagorn, L., 2003. Acoustics for ecosystem research: lessons and perspectives from a scientific programme focusing on tuna environment relationships. Aquat. Living Resour. 16, 197–203.
Bigg, G.R., 1992. Validation of trends in the surface wind field over the Mozambique Channel. Int. J. Climatol. 12, 829–838.
Chelton, D.B., Schlax, M.C., Samelson, R.M., De Szoeke, R.A., 2007. Global observations of large oceanic eddies. Geophys. Res. Lett. 34, 1–5.
Chelton, D., Schlax, M., Samelson, R., 2011. Global observations of nonlinear mesoscale eddies. Prog. Oceanogr. 91, 167–216.
De Ruijter, W., Ridderinkhof, H., Lutjeharms, J., Schouten, M., Veth, C., 2002. Observations of the flow in the Mozambique Channel. Geophys. Res. Lett. 29, 1502.
De Ruijter, W., Van Aken, H., Beier, E., Lutjeharms, J., Matano, R., Schouten, M., 2004. Eddies and dipoles around South Madagascar: formation, pathways and large-scale impact. Deep-Sea Res. I 51, 383–400.
Domokos, R., 2009. Environmental effects on forage and longline fishery performance for albacore (Thunnus alalunga) in the American Samoa Exclusive Economic Zone. Fish. Ocean 18, 419–438.
Domokos, R., Seki, M.P., Polovina, J.J., Hawn, D.R., 2007. Oceanographic investigation of the American Samoa albacore (Thunnus alalunga) habitat and longline fishing grounds. Fish. Ocean 16, 555–572.
Drazen, J.C., De Forest, L.G., Domokos, R., 2011. Micronekton biomass and biomass in Hawaiian waters as influenced by seamounts, eddies, and the moon. Deep-Sea Res. II 58, 557–566.
Foote, K.G., Knudsen, H.P., Vestnes, G., MacLennan, D.N., Simmonds, E.J., 1987. Calibration of acoustic instruments for fish density estimation: a practical guide. ICES J. Mar. Sci. 144, 1–69.
Franks, P.J.S., Wroblewski, J.S., Flierl, G.R., 1986. Prediction of phytoplankton growth in response to the frictional decay of a warm-core ring. J. Geophys. Res. 91, 7603–7610.
Godø, O.R., Patel, R., Pedersen, G., 2009. Diel migration and swimbladder resonance of small fish: some implications for analyses of multifrequency echo data. ICES J. Mar. Sci. 66, 1143–1148.
Godø, O.R., Samuelsen, A., Macaulay, G.J., Patel, R., Hjøllo, S.S., et al., 2012. Mesoscale Eddies Are Oases for Higher Trophic Marine Life. PLoS ONE 7 (1), e30161, http://dx.doi.org/10.1371/journal.pone.0030161.
Goldthwait, S.A., Steinberg, D.K., 2008. Elevated biomass of mesozooplankton and enhanced fecal pellet flux in cyclonic and mode-water eddies in the Sargasso Sea. Deep-Sea Res. II 55, 1360–1377.
Gruber, N., Lachkar1, Z., Frenzel, H., Marchesiello, P., Münnich1, M., McWilliams, J.C., Nagai, T., Plattner, G., 2011. Eddy-induced reduction of biological production in eastern boundary upwelling systems. Nat. Geosci. 4, 787–792.
Halo, I., Backeberg, B., Penven, P., Ansorge, I., Reason, C., Ulgren, J., 2013. Eddy properties in the Mozambique Channel: a comparison between observations and two numerical ocean circulation models. Deep-Sea Res. II.
Huggett, J., 2013. Mesoscale distribution and community composition of zooplankton in the Mozambique Channel. Deep-Sea Res. II.
Hyrenbach, K.D., Veit, R.R., Weimerskirch, H., Hunt, G.L., 2006. Seabird associations with mesoscale eddies: the subtropical Indian Ocean. Mar. Ecol. Prog. Ser. 324, 271–279.
José, Y.S., Aumont, O., Machu, E., Penven, P., Moloney, C.L., Maury, O., 2013. Influence of mesoscale eddies on biological production in the Mozambique Channel: several contrasted examples from a coupled ocean-biogeochemistry model. Deep-Sea Res. II.
Kim, D., Yang, E.J., Kim, K.H., Shin, C-W., Park, J., Yoo, S., Hyun, J-H., 2011. Impact of an anticyclonic eddy on the summer nutrient and chlorophyll a distributions in the Ulleung Basin, East Sea (Japan Sea). ICES J. Mar. Sci. 69, 23–29.
Kloser, R.J., Ryan, T.E., Young, J.W., Lewis, M.E., 2009. Acoustic observations of micronekton fish on the scale of an ocean basin: potential and challenges. ICES J. Mar. Sci. 66, 998–1006.
Kolasinski, J., Kaehler, S., Jaquemet, S., 2012. Distribution and sources of particulate organic matter in a mesoscale eddy dipole in the Mozambique Channel (south-western Indian Ocean): Insight from C and N stable isotopes. ICES J. Mar. Sci. 96–97, 121–131.
Korneliussen, R.J., Diner, N., Ona, E., Berger, L., Fernandes, P.G., 2008. Proposals for the collection of multifrequency acoustic data. ICES J. Mar. Sci. 65, 982–994.
Lambardi, P., Lutjeharms, J.R.E., Mencacci, R., Hays, G.C., Luschi, P., 2008. Influence of ocean currents on long-distance movement of leatherback sea turtles in the Southwest Indian Ocean. Mar. Ecol. Prog. Ser. 353, 289–301.
Lamont, T., Barlow, R., Morris, T., Van den Berg, M., 2013. Characterisation of mesoscale features and phytoplankton variability in the Mozambique Channel. Deep-Sea Res. II.
Landry, M.R., Decima, M., Simmons, M., Hannides, C.C.S., Daniels, E., 2008. Mesozooplankton biomass and grazing responses to Cyclone Opal, a subtropical mesoscale eddy. Deep-Sea Res. II 55, 1378–1388.
Lawson, G.L., Wiebe, P.H., Stanton, T.K., Ashjian, C.J., 2008. Euphausiid distribution along the Western Antarctic Peninsula - Part A: development of robust multi-frequency acoustic techniques to identify euphausiid aggregations and quantify euphausild size, abundance, and biomass. Deep-Sea Res. II 55, 412–431.
Lebourges-Dhaussy, A., Huggett, J., Ockhuis, S., Roudaut, G., Josse, E., Verheye, H., 2013. Zooplankton size and distribution within mesoscale structures in the Mozambique Channel: a comparative approach using the TAPS acoustic profiler, a multiple net sampler and ZooScan image analysis. Deep-Sea Res. II.
Lebourges-Dhaussy, A., Marchal, E., Menkès, C., Champalbert, G., Biessy, B., 2000. Vinciguerria nimbaria (micronekton), environment and tuna: their relationships in the Eastern Tropical Atlantic. Oceanol. Acta 23, 515–528.
Lurton, X., 2002. An Introduction to Underwater Acoustics: Principles and Applications. © Praxis, Chichester, UK.
MacLennan, D.N., Fernandes, P.G., Dalen, J., 2002. A consistent approach to definitions and symbols in fisheries acoustics. ICES J. Mar. Sci. 59, 365–369.
Malauene, B.S., Shillington, F.A., Roberts, M.J., Moloney, C.L., 2013. Cool, elevated-chlorophyll *a* waters off northern Mozambique. Deep-Sea Res. II.
McGillicuddy Jr., D.J., Anderson, L.A., Bates, N.R., Bibby, T., Buesseler, K.E., Carlson, C.A., Davis, C.S., Ewart, C., Falkowski, P.G., Goldthwait, S.A., Hansell, D.A., Jenkins, W.J., Johnson, R., Kosnyrev, V.K., Ledwell, J.R., Li, Q.P., Siegel, D.A., Steinberg, D.K., 2007. Eddy/wind interactions stimulate extraordinary mid-ocean plankton blooms. Science 316, 1021–1026.
McGillicuddy Jr., D.J., Robinson, A.R., 1997. Eddy-induced nutrient supply and new production in the Sargasso Sea. Deep-Sea Res. I 44, 1427–1450.
McGillicuddy Jr., D.J., Robinson, A.R., Siegel, D.A., Jannasch, H.W., Johnson, R., Dickey, T.D., McNeil, J., Michaels, A.F., Knap, A.H., 1998. Influence of mesoscale eddies on new production in the Sargasso Sea. Nature 394, 263–266.
Mehner, T., Kasprzak, P., 2011. Partial diel vertical migrations in pelagic fish. J. Anim. Ecol. 80, 761–770.

Ménard, F., Benivary, H.D., Bodin, N., Coffineau, N., Le Loc'h, F., Misona, T., Richard, P., Potier, M., 2013. Stable isotope patterns in micronekton from the Mozambique Channel. Deep-Sea Res. II.
Ménard, F., Marchal, E., 2003. Foraging behaviour of tuna feeding on small schooling Vinciguerria nimbaria in the surface layer of the equatorial Atlantic Ocean. Aquat. Living Resour. 16, 231–238.
Mizobata, K., Saitoh, S.I., Shiomoto, A., Miyamura, T., Shiga, N., Imai, K., Toratani, M., Kajiwara, Y., Sasaoka, K., 2002. Bering Sea cyclonic and anticyclonic eddies observed during summer 2000 and 2001. Prog. Oceanogr. 55, 65–75.
Muhling, B.A., Beckley, L.E., Olivar, M.P., 2007. Ichthyoplankton assemblage structure in two meso-scale Leeuwin Current eddies, eastern Indian Ocean. Deep-Sea Res. II 54, 1113–1128.
Nel, D.C., Lutjeharms, J.R.E., Pakhomov, E.A., Ansorge, I.J., Ryan, P.G., Klages, N.T.W., 2001. Exploitation of mesoscale oceanographic features by grey-headed albatross Thalassarche chrysostoma in the southern Indian Ocean. Mar. Ecol. Prog. Ser. 217, 15–26.
Olsson, I.C., Greenberg, L.A., Bergman, E., Wysujack, K., 2006. Environmentally induced migration: the importance of food. Ecol. Let. 9, 645–651.
Polovina, J.J., Balazs, G.S., Howell, E.A., Parker, D.M., Seki, M.P., Dutton, P.H., 2004. Forage and migration habitat of loggerhead (Caretta caretta) and olive ridley (Lepidochelys olivacea) sea turtles in the central North Pacific Ocean. Fish. Ocean 13, 36–51.
Potier, M., Bach, P., Ménard, F., Marsac, F., 2013. Influence of mesoscale features on micronekton and large pelagic fish communities in the Mozambique Channel. Deep-Sea Res. II.
Quartly, G.D., Srokosz, M.A., 2004. Eddies in the southern Mozambique Channel. Deep-Sea Res. II 51, 69–83.
Ramage, C.S., 1969. Indian Ocean surface meteorology. Oceanogr. Mar. Biol. 7, 11–30.
R Development Core Team, 2007. R: A Language and Environment for Statistical Computing. R Foundation for Statistical Computing, Vienna, Austria.
Roberts, M.J., Ternon, J-F., Morris, T., 2013. Interaction of (dipole) eddies with the western continental slope of the Mozambique Channel. Deep-Sea Res. II.
Roger, C., Grandperrin, R., 1976. Pelagic food webs in the tropical Pacific. Limnol. Oceanogr. 21, 731–735.
Sabarros, P.S., Ménard, F., Lévénez, J.J., Tew-Kai, E., Ternon, J-F., 2009. Mesoscale eddies influence distribution and aggregation patterns of micronekton in the Mozambique Channel. Mar. Ecol. Prog. Ser. 395, 101–107.
Schott, F.A., McCreary Jr., J.P., 2001. The monsoon circulation of the Indian Ocean. Prog. Oceanogr. 51, 1–123.
Schouten, M., De Ruijter, W., Van Leeuwena, P.J., Ridderinkhof, H., 2003. Eddies and variability in the Mozambique Channel. Deep-Sea Res. II 50, 1987–2003.
Seki, M.P., Polovina, J.J., Kobayashi, D.R., Bidigare, R.R., Mitchum, G.T., 2002. An oceanographic characterization of swordfish (Xiphias gladius) longline fishing grounds in the springtime subtropical North Pacific. Fish. Ocean 11, 251–266.
Siegel, D.A., Peterson, P., McGillicuddy Jr., D.J., Maritorena, S., Nelson, N.B., 2011. Bio-optical footprints created by mesoscale eddies in the Sargasso Sea. Geophys. Res. Lett. 38, 1–6.
Simmonds, J., MacLennan, D., 2005. Fisheries Acoustics: Theory and Practice, second ed. Blackwell Science, Oxford.
Simrad, 2008. Simrad ER60, Scientific echo sounder. Reference Manual, Release 2.2.0., Kongsberg Maritime AS, Kongsberg, Norway.
Strzelecki, J., Koslow, J.A., Waite, A., 2007. Comparison of mesozooplankton communities from a pair of warm- and cold-core eddies off the coast of Western Australia. Deep-Sea Res. II 54, 1103–1112.
Ternon, J-F., Bach, P., Barlow, R., Huggett, J., Jaquemet, S., Marsac, F., Menard, F., Penven, P., Potier, M., Roberts, M., 2013a. The Mozambique Channel: from physics to upper trophic levels. Deep-Sea Res. II.
Ternon, J-F., Roberts, M.J., Morris, T., Hancke, L., Backeberg, B., 2013b. In situ measured current structures of the eddy field in the Mozambique Channel. Deep-sea Res. II.
Tew-Kai, E., Marsac, F., 2009. Patterns of variability of sea surface chlorophyll in the Mozambique Channel: a quantitative approach. J. Mar. Syst. 77, 77–88.
Tew-Kai, E., Marsac, F., 2010. Influence of mesoscale eddies on spatial structuring of top predators' communities in the Mozambique Channel. Prog. Oceanogr. 86, 214–223.
Venables, W.N., Ripley, B.D., 2002. Modern Applied Statistics with S, fourth ed. Springer-Verlag, New York.
Watanabe, H., Kubodera, T., Moku, M., Kawaguchi, K., 2006. Diel vertical migration of squid in the warm core ring and cold water masses in the transition region of the western North Pacific. Mar. Ecol. Prog. Ser. 315, 187–197.
Watanabe, H., Moku, M., Kawaguchi, K., Ishimaru, K., Ohno, A., 1999. Diel vertical migration of myctophid fishes (Family Myctophidae) in the transitional waters of the western North Pacific. Fish. Oceanogr. 8, 115–127.
Weill, A., Scalabrin, C., Diner, N., 1993. MOVIES-B: an acoustic detection description software. Application to shoal species' classification. Aquat. Living Resour. 6, 255–267.
Weimerskirch, H., Le Corre, M., Jaquemet, S., Potier, M., Marsac, F., 2004. Foraging strategy of a top predator in tropical waters: great frigatebirds in the Mozambique Channel. Mar. Ecol.. Prog. Ser. 275, 297–308.
Young, J.W., Bradford, R., Lamb, T.D., Clementson, L.A., Kloser, R., Galea, H., 2001. Yellowfin tuna (Thunnus albacares) aggregations along the shelf break off south-eastern Australia: links between inshore and offshore processes. Mar. Freshw. Res. 52 (4), 463–474.
Zimmerman, R.A., Biggs, D.C., 1999. Patterns of distribution of sound-scattering zooplankton in warm- and cold-core eddies in the Gulf of Mexico, from a narrowband acoustic Doppler current profiler survey. J. Geophys. Res. 104, 5251–5262.